Proceedings of the Ninth EGS4 Users' Meeting in Japan, KEK Proceedings 2001-22, p.108-114

COUNT RATE PERFORMANCE SIMULATIONS FOR NEXT GENERATION 3D PET SCANNERS

K. Kitamura[1,2] and H. Murayama[2]

[1] *Medical Systems Division, Shimadzu Corporation*
1 Nishinokyo-Kuwabaracho, Nakagyo-ku, Kyoto-shi, Kyoto 604-8511, Japan
[2] *Department of Medical Physics, National Institute of Radiological Sciences*
9-1 Anagawa-4, Inage-ku, Chiba-shi, Chiba 263-8555, Japan

Abstract

The design goal of next generation PET scanners is to increase both spatial resolution and system sensitivity. Detectors capable of depth-of-interaction (DOI) measurement can increase sensitivity by increase scanner geometrical efficiency without degrading spatial resolution. However, reducing the detector ring diameter leads to the increase in scatter and random coincidences along with true coincidences, and may affect system count rate performance. Thus the assessment of the effect of changing the geometry of 3D PET scanners on count rate performance was made using EGS4 Monte Carlo simulation and count rate model calculation. Computed count rates have good agreement with those of the current PET scanners. Similar computation predicts that 3D PET scanners with the GSO DOI detectors using a large area PS-PMT will have higher sensitivity and noise equivalent count rates than those of the current PET system. But reducing the scanner diameter will increase singles flux per detector, which contributes to the dead time of the scanner, and may require additional data acquisition electronics.

1 Introduction

In order to develop molecular imaging techniques that use radiolabeled tracers to image biological processes in vivo, a next generation PET camera capable of high sensitivity and high resolution is now under design at National Institute of Radiology (NIRS). The sensitivity of a 3D PET scanner is directly related to the integral of the solid angle subtended by the detectors over the source distribution. Detectors with the depth-of-interaction (DOI) capability can minimize the effect of the crystal penetration of obliquely incident gamma rays even in scanners with high geometrical efficiency (small detector ring diameter and large axial FOV), which can increase system sensitivity while maintaining high spatial resolution. At NIRS, a DOI detector with Gd_2SiO_5 (GSO) crystals coupled to a position-sensitive photomultiplier tube (PS-PMT) was designed and evaluated [1], in which DOI information can be extracted from the ratio of anode signals from the PS-PMT using standard Anger-type positioning.

In PET studies, count rate performance is an important factor to affect the reconstructed image quality. Placing the detector modules closer to the patient requires detectors with high count rate performance to minimize dead time losses [2][3]. On the other hand, faster decay and high light yield properties of GSO scintillator improve energy and time resolution, which may result in the decrease in scatter and random coincidences. We therefore estimated the count rate performance

of the GSO-DOI PET scanners with different geometry using EGS4 Monte Carlo simulations and count rate model calculation.

2 Monte Carlo Simulation

In this work, Monte Carlo simulation programs based upon EGS4 were used to calculate photon interactions in the scintillation crystals and uniform cylindrical phantoms [4][5]. Fig.1 shows the geometry of the simulated phantom and detectors. To account for detector packing fraction, discrete rectangular detector blocks separately arranged are modeled. Two annihilation photons are generated and Compton and Rayleigh scattering in a phantom are simulated. Photons escaped from the phantom are recorded with their position, direction, energy, and the number of scattering. The direction and position of the photon are used to determine the incident detector k, and are converted to the detector coordinate system (X_k, Y_k, Z_k). After that, Compton and photoelectric interactions within the scintillator are tracked and recorded for each incident photon if the interactions are occurred. If the gamma ray is escaped to the adjacent detector, their position and direction are converted to the new detector coordinate and successive interactions are simulated. No attempt was made to simulate the crystal spacing with inner reflectors and the detector casing

The energy response was modeled by a Gaussian distribution of the detected photon energy. If the total energy deposited at each detector block is within an energy window, the event is recorded as a 'post-window' single event, which in part became a random coincidence. If the energy is higher than the threshold of the discriminator activating the PMT pulse integrator which determine the position and energy of the incident photon, the event is also recorded as a 'pre-window' single event. A pair of photons having the same annihilation tag is counted as a coincidence event, and is considered as a scatter coincidence when either of photon has a non-zero scattering flag. A random coincidence count rate Rij for a detector pair (i, j) is given by $R_{ij} = 2\tau N_i N_j$, where 2τ is a coincidence time window and N_i, N_j are single count rates of detector i, j.

3 Count Rate Model

Since the proposed DOI detector unit does not require additional electronics and photo-detectors, dead-time factors at each level of the data acquisition system can be calculated using a conventional count rate model [6] as a function of activity concentrations. The number of 'pre-window' single events is used to calculate the dead time at the front-end circuits. The outputs of the front-end circuits, which are 'post-window' single events, are grouped into buckets via OR-logic. True, scatter and random coincidence events are presented to the coincidence processors for each bucket pair and then transferred to the acquisition memory through the encoder. At each level described above, the count losses of events are calculated according to the system dead time. We applied a paralyzable dead time for the front-end circuit and a non-paralyzable dead time for the other circuits.

4 Validation

Validation of the simulation program was performed by comparing calculated count rates with those measured on a Shimadzu Headtome-V (SET-2000W series) PET scanner [7]. Headtome-V has 112 $Bi_4Ge_3O_{12}$ (BGO) detector blocks per ring (each size of 22.8 mm tansaxially $\times$ 50 mm axially $\times$ 30 mm radially), and three types of the axial FOV: 20 cm (SET-2400W), 15 cm (SET-2300W), and 10 cm (SET-2200W). These all have the same acquisition electronics except for the size of the acquisition memory. Measurement was made with a ϕ420 cm $\times$ 20 cm cylinder filled

with a uniform activity distribution in a SET-2400W scanner and a ϕ 14 cm $\times$ 15 cm in SET-2200W and SET-2300W scanners. Fig.3 shows the simulated and measured count rates versus activity concentration. These results indicate that the agreements are good enough to predict system count rate performance for different scanner and phantom geometry. Considering the fact that the measured count rates tend to be easily affected by the detector conditions, the count rate model used in this simulation is reasonable.

5 Next Generation PET Scanners

For the new generation of 3D PET scanners, we assumed that the detector unit consists of 8×8 crystal blocks coupled to a 52 mm squire PS-PMT [8] having 16×16 multi-anodes (Fig. 2). Each block consists of four stages of 2×2 crystal arrays and each position of the 256 bottom crystal elements corresponds to that of each anode segment. The position of a crystal element detecting a gamma photon is determined by applying Anger-type position arithmetic to the output signals from the PMT anodes.

Table 1 describes scanner parameters with different geometry having almost the same geometrical efficiency at the center of the FOV. All the stages of the detector elements were assumed to have the same energy resolution of 20% with an integration time of 250 ns. A lower energy level discriminator setting of 200 keV and an energy window of 400-600 keV was simulated. The assumptions were made that a coincidence time-window was 6 ns, and the bandwidth of the encoder was 20 MHz.

A ϕ20 cm $\times$ 20 cm water phantom filled with a uniform activity distribution placed at the center of the scanner were simulated. Sensitivity is defined as the ratio of the true coincidence rate to the activity concentration at low dead time level, and scatter fraction is defined as the ratio of the scatter coincidence rate to the total coincident rate. The scanner A, B and C have a sensitivity of 144, 116, and 103 kcps/kBq/ml with a scatter fraction of 35.4, 36.3, and 37.3%, respectively.

Noise equivalent count rates NECR = $T^2/(T+S+fR)$ were also calculated, where T is the total true coincidence rate and S and R are the scatter and random coincidence rates and f is the ratio of the lines of response passing through the object, assumed that the estimate of the random coincidence rate is noise-free. Figure 4 shows the calculated true and random coincidence rates and NECR. For the scanner A, a maximum NECR of 760 kcps is obtained with activity densities of 15 kBq/ml. Thus, the proposed design has roughly a factor of five higher peak NECR than those of existing scanners, mostly due to the high geometrical efficiency and time resolution.

However, NECR for the scanner with a smaller diameter is rapidly saturated and its maximum is less than half that of scanner A. As show in Fig. 6, single rate per detector block of scanner C is much higher than those of scanner A, while both coincidence rates per buckets are almost the same (Fig. 5). These results suggest that the NECR of these small diameter scanners can be improved by the additional electronics, in which subset anode signals from the PS-PMT are independently read out and processed.

6 Discussion and Conclusions

Count rate performance simulations using EGS4 have been performed and compared to the current 3D PET scanners. Slight differences between the simulated and measured data are attributed to the fact that the detector tuning parameters, the gantry shield and the detector casing were not simulated.

Our preliminary simulations show that the 3D PET scanner with the GSO-DOI detectors using the large area PS-PMT will have high sensitivity and high count rate performance compared with the current PET scanners. For scanners with a smaller ring diameter, there is a possibility to

further increase NECR by parallel processing of subset signals from the PS-PMT to address the increase in single event rates. Since NEC rates have been shown to be strongly dependent on object size and tracer distribution, further simulations are necessary to investigate the optimal scanner design.

References

1) H. Murayama, H. Ishibashi, H. Uchida, T. Omura, T. Yamashita, "Design of a Depth of Interaction Detector with a PS-PMT for PET," *IEEE Trans. Nucl. Sci.* **NS-47** (2000)1045-1050.

2) W. W. Moses, P. R. G. Virador, S. E. Derenzo, R. H. Huesman, T. F. Budinger, "Design of a High - Resolution, High - Sensitivity PET Camera for Human Brains and Small Animals," *IEEE Trans. Nucl Sci.* **NS-44**(1997)1487 - 1491.

3) R. D. Badawi, S. G. Kohlmyer, R. L. Harrison, S. D. Vannoy, T. K. Lewellen, "The effect of camera geometry on singles flux, scatter fraction and trues and randoms sensitivity for cylindrical 3D PET -a simulation study," *IEEE Trans. Nucl. Sci.* **NS-47** (2000)1228-1232.

4) Y. Narita, M. Shidahara, T. Nakamura, T. Fujiwara, M. Itoh, "Simulation of Compton scatter in 3-Dimentional PET," Proceedings of the First International Workshop on EGS4, *KEK Proceeding 97-16*, pp. 174-180, 1997.

5) L. E. Adam and J. S. Karp, "Optimization of PET scanner geometry," Proceedings of the Second International Workshop on EGS4, *KEK Proceeding 2000-20*, pp. 92-99, 2000.

6) C. Moisan, J. G. Rogers, J. L. Douglas, "A count rate model for PET and its Application to an LSO HR PLUS scanner," *IEEE Trans. Nucl. Sci.* **NS-44**(1997)1219-1224.

7) T. Fujiwara, S. Watanuki, S. Yamamoto, M. Miyake, S. Seo, M. Itho, K. Ishii, H. Orihara, H. Fukuda, T. Satoh, K. Kitamura, K. Tanaka, S. Takahashi, "Performance evaluation of a large axial field-of-view PET scanner: SET-2400W," *Annals of Nuclear Medicine* **Vol. 11, No .4**(1997)307-313.

8) H. Kyushima, H. Simoi, A. Atsumi, Y. Yoshizawa, "The Development of Flat Panel PMT," *2000 IEEE NSS & MIC Conf. Rec.* Lyon, 2001.

Table 1 Scanner parameters with different geometry (A,B,C)

	A	B	C
scanner diameter [cm]	60.0	47.7	38.2
scanner length [cm]	40.0	30.0	25.8
geometrical efficiencyat at the center of the FOV	0.55	0.53	0.54
number of ring blocks	8	6	5
number of blocks per ring	38	30	24
number of buckets	19	15	12
number of coincidence bucket pairs	95	60	42

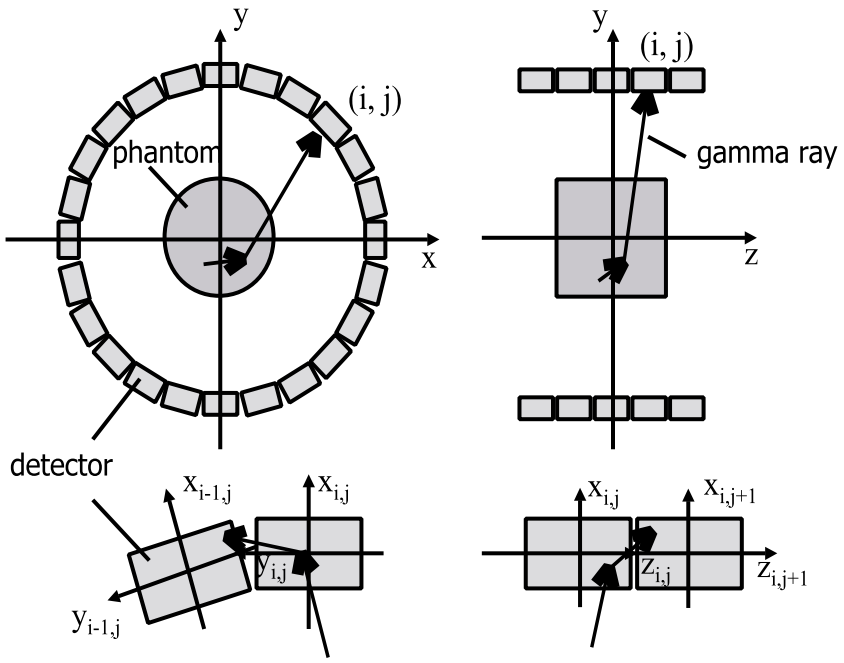

Figure 1: PET scanner and detecctor coordinate system. Left) frontal view, Right) axial cross section.

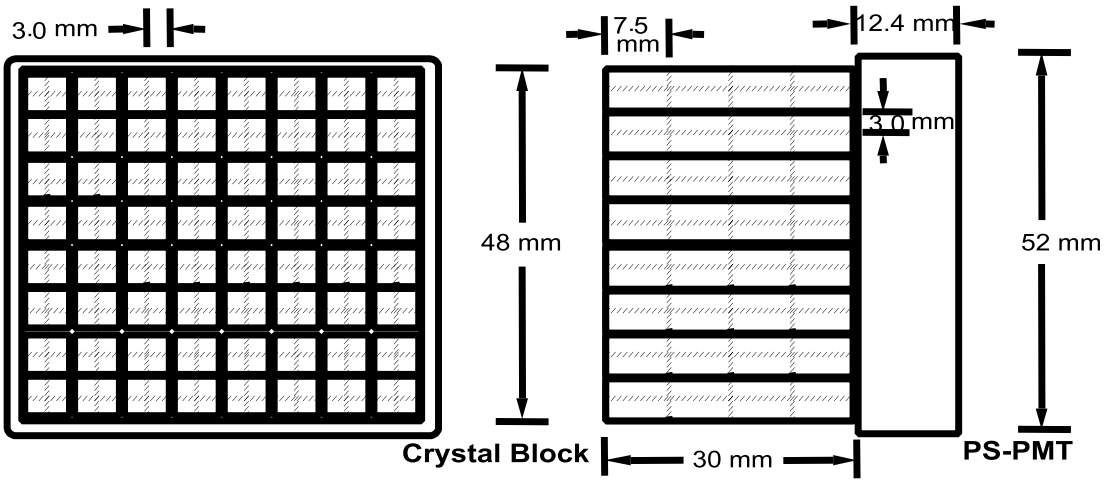

Figure 2: Schematic representation of the detector module.

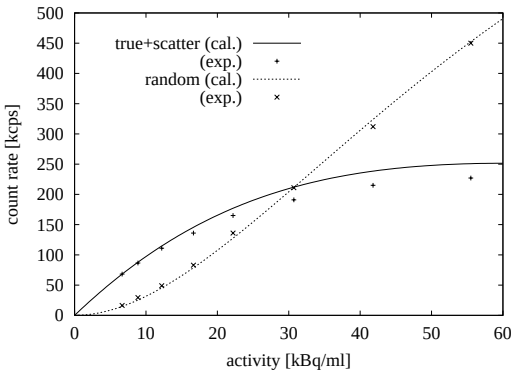

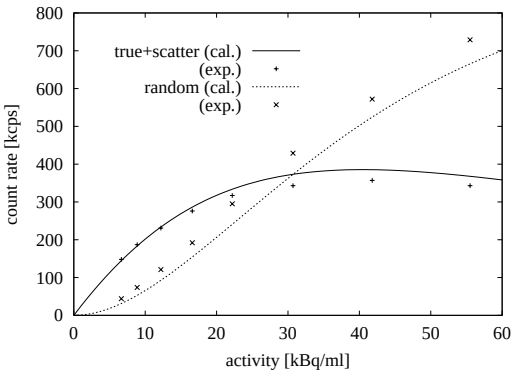

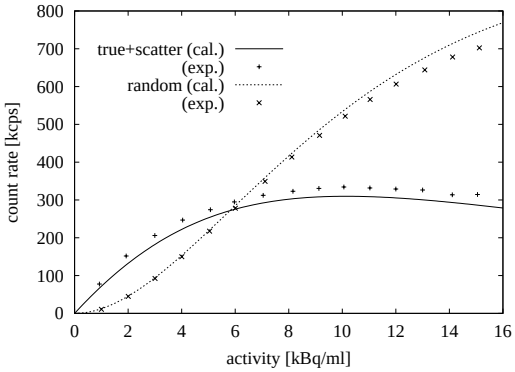

Figure 3: Comparison of measured (symbols) and calculated (lines) count rate performance of the SET-2200W (top left), SET-2300W (top right), and SET-2400W (bottom left).

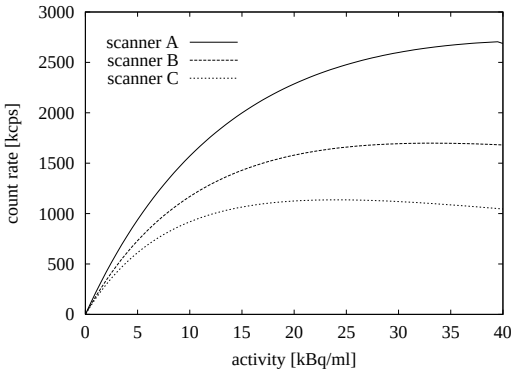

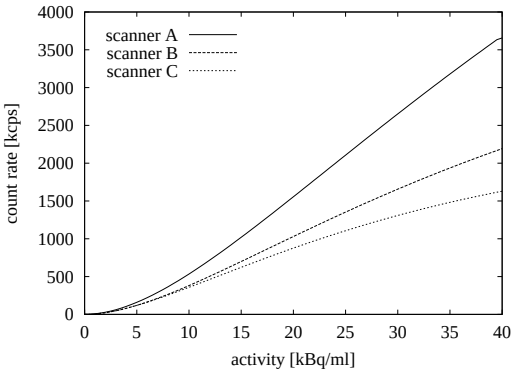

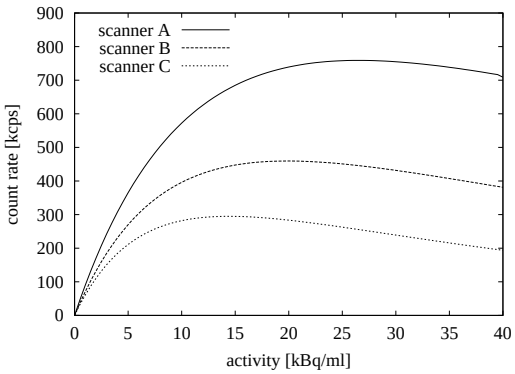

Figure 4: Predicted true coincidence (top left), random coincidence (top right), and NECR curves (bottom left) for the scanners with different geometry described in Table 1.

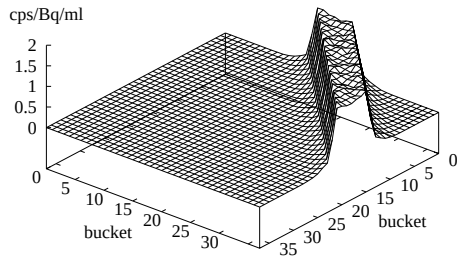

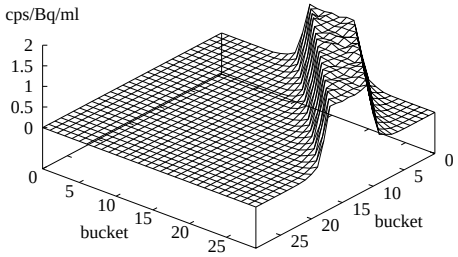

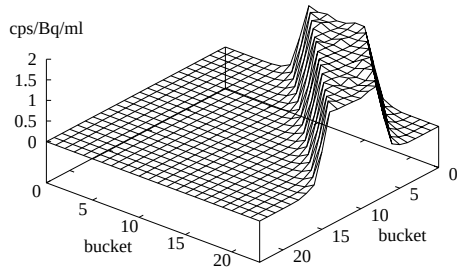

Figure 5: True and scatter coincidence rates per bucket pair for the scanner A (top left), B (top right), and C (bottom left).

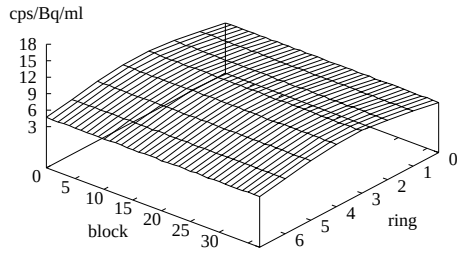

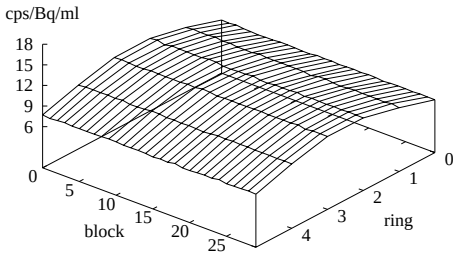

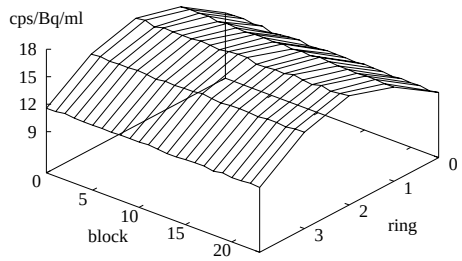

Figure 6: Single count rates per detector block for the scanner A (top left), B (top right), and C (bottom left).